Inorganic Chemistry

Article

pubs.acs.org/IC

Bond Network Topology and Antiferroelectric Order in Cuprice CuOH

Yunguo Li,[†] Cláudio M. Lousada,[†] Inna L. Soroka,[‡] and Pavel A. Korzhavyi*[,†]

[†]Department of Materials Science and Engineering and [‡]Applied Physical Chemistry, School of Chemical Science and Engineering, Royal Institute of Technology (KTH), S-100 44 Stockholm, Sweden

Supporting Information

ABSTRACT: Using density functional theory (DFT) and a graph theory based approach, we investigated the topology of bond network in CuOH(s) (cuprice) considering only symmetry-distinct structures. In parallel, we conducted the synthesis and X-ray diffraction characterization of the compound and used the combined theoretical–experimental effort to validate the lowest energy structure obtained with DFT. The ground-state structure of CuOH(s) consists of compact trilayers of CuOH connected to each other via hydrogen bonds, where the inner layer of each trilayer is composed entirely of Cu atoms. Each trilayer is a dense fabric made of two interlocked arrays of polymer $[CuOH]_n$ chains. This structure corresponds to an antiferroelectric configuration where the dipole moments of CuOH molecules belonging to adjacent arrays are antiparallel and are arranged in the same way as the water molecules in ice-VIII. It is shown that a collective electrostatic interaction is the main driving force for the cation ordering while the local atomic configuration is maintained. These findings and the possibility of synthesizing exfoliated two-dimensional cuprice are important for some technological applications.

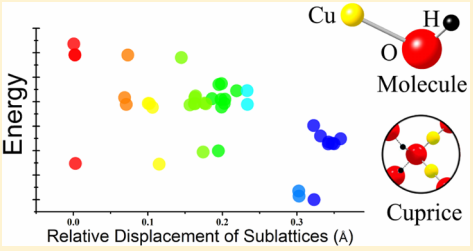

INTRODUCTION

The interactions of water with metal surfaces play essential roles in fields such as catalysis, electrochemistry, and corrosion and have important applications in, for example, hydrogen production, microelectronics, and fuel cells.[1,2] A variety of low-dimensional structures can be formed on metal surfaces with increased water adsorption. Water adsorption on Cu(110) and Cu(100) surfaces is known to occur via a dissociative pathway,[3,4] and water–hydroxyl dimers and chains were recently observed in studies that used scanning tunneling microscopy (STM).[5−8] However, the question whether the hydration and hydroxylation of copper are limited to the surface, or if they can proceed into the bulk, remains open.[9,10] This question is critical for a number of technological applications, including the application of copper as a canister material for long-term storage of spent nuclear fuel.[11] Because hydroxides are typical products of water–metal reactions, understanding the formation of solid CuOH and its structure and thermodynamic stability may elucidate the role of CuOH in the interaction of metallic copper with an aqueous environment.

The structure of the solid form of cuprous hydroxide is unknown and is often referred to as CuOH amorphous.[9,10] The principles of atomic coordination in solid-state CuOH were established in a recent theoretical study,[12] and the structure proposed then was named "cuprice", to address its structural resemblance to Cu_2O cuprite and H_2O ice.

The proposed structure of cuprice is intermediate between the crystal structures of cuprite and ice-VII (the latter consists of two interpenetrating lattices of cubic ice I_C). Cuprice CuOH shares a similar oxygen framework with cuprite Cu_2O and ice-VII, as shown in Figure 1. The coordination of cuprous cations and protons in cuprice CuOH is similar to the coordination of these ions in cuprous oxide Cu_2O (cuprite) and ice H_2O, respectively.[12] The mixture between the Cu_2O and H_2O structures may be viewed as a more or less random cation substitution of H for Cu in Cu_2O to form CuOH, which also explains why it is so difficult to experimentally distinguish cuprice from cuprite or from the structures of possible hydrated

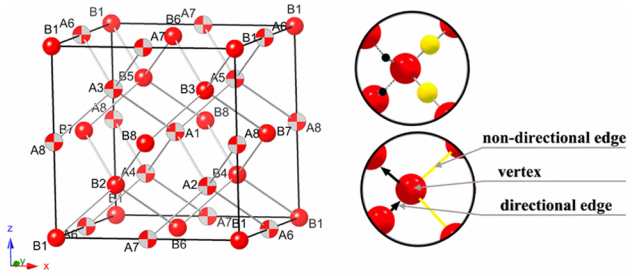

Figure 1. (left) Oxygen framework in Cu_2O, ice-VII/VIII, and cuprice CuOH. The lattice contains two identical interpenetrating sublattices (labeled as A and B). Dashed lines indicate either the O–Cu–O bond or the O–H···O bond depending on the material. (top right) O–Cu–O and O–H···O bonds in CuOH, which are represented by the nondirectional edge and directional edge, respectively, in the figure below.

Received: May 13, 2015
Published: September 3, 2015

DOI: 10.1021/acs.inorgchem.5b01030
Inorg. Chem. 2015, 54, 8969–8977

Table 1. Adjacency List of Topology of Bond Network in Cuprice[a]

	A1/Bl	A2/B2	A3/B3	A4/B4	A5/B5	A6/B6	A7/B7	A8/B8
A1/B1	*	1	1	1	1	0	0	0
A2/B2	1	*	0	0	0	1	1	1
A3/B3	1	0	*	0	0	1	1	1
A4/B4	1	0	0	*	0	1	1	1
A5/B5	1	0	0	0	*	1	1	1
A6/B6	0	1	1	1	1	*	0	0
A7/B7	0	1	1	1	1	0	*	0
A8/B8	0	1	1	1	1	0	0	*

[a]A and B denote the different sublattices as shown in Figure 1, and the number labels of the atoms are given in Figure 1. The value 1 denotes adjacent, and 0 denotes disconnected.

forms of cuprous oxide or hydroxide (all of these compounds can generally be denoted as $Cu_2O{\cdot}nH_2O$, $0 \le n \le 3$).[13]

Oxides and hydroxides may incorporate high degrees of configurational disorder that is amenable to a mathematical treatment similar to the proton disorder in water ice.[14−16] A high degree of cation disorder could be expected in CuOH, if all the configurations not breaking the so-called Pauling ice rules were strictly, or nearly, degenerate in energy. This assumed degeneracy was not proved for CuOH; thus, it is necessary to investigate whether the topology of the bond network has an effect on the total energy of cuprice. Similarly, the hydrogen bond (HB) topology in water ice has for a long time been assumed to have no effect on the total energy. Recent studies have revealed that the ice structures with different HB topologies are not strictly degenerate but differ at most by about 1 kJ/mol per H_2O.[15−18] In spin ice systems, which generally obey the Pauling ice rule,[19] the degeneracy can be lifted due to magnetic dipole interactions.[20]

In this work we employ ab initio calculations based on density functional theory (DFT) to study the relationship between the topology of the bond network and the total energy of various cation configurations of CuOH, with the aim to determine the lowest-energy structure of cuprice and to accurately estimate its thermodynamic properties. X-ray diffraction measurements of cuprous hydroxide powder, synthesized via a wet chemical route, are employed to verify the theoretically obtained structure.

METHODOLOGY

Total Amount of Disorder. Let us first evaluate the maximum configurational entropy associated with the distribution and positioning of protons, according to the Pauling ice rule,[14] in the cation-disordered CuOH structure. The structure consists of two interpenetrating lattices; each of these is based on a cubic diamond sublattice of oxygen (Figure 1). Every anion is tetrahedrally coordinated by two copper cations and two protons, while every cation is linearly coordinated by two oxygen anions. The distribution of Cu and H cations gives rise to the same configurational entropy (per mole of CuOH) as that of H_2O ice, as first evaluated by Pauling:[14]

$$S_0(H_2O) = R \ln\left(\frac{3}{2}\right) = 3.37\ \mathrm{J/(mol\,K)} \quad (1)$$

where S_0 is the configurational entropy and R the ideal gas constant.

In addition, the structure of CuOH possesses proton disorder: of the two hydrogens neighboring every oxygen anion, one is tightly bound to the anion (bond length is 0.973 Å), while the other is connected to it by a longer hydrogen bond (2.204 Å). Copper cations are situated midway between the two neighboring anions and thus do not further contribute to the entropy. A random displacement of N protons toward the anions would increase the number of configurations in a cuprice crystal containing N CuOH molecules by a factor of 2^N. However, this number must be reduced (by a factor of $2^{N/2}$) to exclude the configurations where none or both of the protons surrounding an oxygen anion are tightly bound to it. The total configurational entropy per one mole of CuOH is thus

$$S_0(\mathrm{CuOH}) = R \ln\left(\frac{3}{\sqrt{2}}\right) = 6.25\ \mathrm{J/(mol\,K)} \quad (2)$$

Hydrated oxide represents another, more ordered, possibility of mixing together the structures of cuprite and cubic ice. In this case, one of the two anticristobalite lattices in the Cu_2O structure is replaced by the crystal lattice of cubic H_2O ice. The lattice of the oxide is fully ordered, while the lattice of ice possesses the same configurational entropy as that of proton-disordered water ice. Thus, the entropy of hydrated cuprous oxide (per 1/2 mol of $Cu_2O{\cdot}H_2O$ formula units) is

$$\frac{1}{2}S_0(Cu_2O{\cdot}H_2O) = \frac{1}{2}S_0(H_2O) = 1.69\ \mathrm{J/(mol\,K)} \quad (3)$$

Structure Enumeration. To investigate the effect of the HB topology on the stability of CuOH, we carried out structural enumeration. In brief, we doubled the size of the simplest unit cell of cuprice[12] along the three spatial directions and explored all possible arrangements (allowed by the Pauling ice rule) of cuprous cations and protons in the thus obtained $2 \times 2 \times 2$ supercell containing 16 CuOH formula units (as shown in Figure 1).

The enumeration of the configurations can be done recurring to graph theory. The topology of the bond network can be summarized by a graph G and expressed by

$$G = \{\{\{A1, A2, ..., A8\}, \{B1, B2, ..., B8\}\}, \{E_A, E_B\}\} \quad (4)$$

where A1, B1, ... indicate vertices (the letter indicates the sublattice, and the number suggests the sequence), i.e. oxygen in our case, and E_A and E_B indicate edges of the two sublattices, respectively. In each sublattice, half the edges are O−Cu−O and the other half are O−H···O. The adjacency list of the graph is shown in Table 1. The oxygen vertices and their labels are shown in Figure 1. The graph contains two identical disconnected subgraphs, and it is only necessary to enumerate one of them. Two types of edges exist in each subgraph, the nondirectional edges E_n representing O−Cu−O and the directional edges E_d representing O−H···O. Each vertex has a degree of 4, being incident with 2 nondirectional edges and 2 directional edges.

On the basis of the adjacency list (Table 1), the number of isomorphs can be evaluated. For one sublattice (for exmple, A) the E_n edges could go through all the vertices in one walk, forming a Hamiltonian circuit (such as A1−A4−A8−A5−A6−A3−A7−A2−A1). At the same time, the E_d edges are forced to form another Hamiltonian circuit (subsequently A1−A3−A8−A2−A6−A4−A7−A5−A1). The second case is where the E_n edges only go through half the vertices in one walk and through the other half in a second walk, forming two cycles (such as A1−A4−A8−A5−A1 and A2−A6−A3−A7−A2). Subsequently, the E_d edges are also forced to form two cycles (namely A1−A2−A8−A3−A1 and A4−A6−A7−A5−A4). Then, the number of

DOI: 10.1021/acs.inorgchem.5b01030
Inorg. Chem. 2015, 54, 8969−8977

isomorphs for each sublattice can be obtained by adding the number of conformations of the two cases:

$$W_\alpha = \frac{4 \times 3 \times 3 \times 2 \times 2}{2} \times 2 + \frac{4 \times 3 \times 3 \times 2}{2} \times 4 = 288 \quad (5)$$

Thus, the number of possible structures in the 2 × 2 × 2 supercell of cuprice is 288^2 = 82944. The total list of structures is highly redundant—but computing the energy for each of them is unnecessary. To enumerate the symmetry-distinct structures, we first enumerate the isomorphs only with E_d edges. From that, 18 symmetry-distinct structures of Cu−O−Cu chains can be obtained. Subsequently the protons must be placed according to the Pauling ice rule. After the symmetry analysis, 40 symmetry-distinct configurations of CuOH were obtained. The ground-state energies of the 40 configurations of the CuOH supercell were then computed in the framework of DFT as described below.

The number of the structures explored by the enumeration above corresponds to a configurational entropy of

$$S_{conf}(\mathrm{CuOH}) = R \ln(288^2)/16 = 5.89\ \mathrm{J/(mol\,K)} \quad (6)$$

which is a bit less than the total configurational entropy of CuOH (eq 2) because of the constraints imposed by the periodic boundary conditions. Thus, the supercell used in the present work allows us to explore most of the possible CuOH configurations.

Computational Details. The calculations are based on DFT and employ a plane-wave basis set, as implemented in the Vienna ab initio simulation package (VASP).[21,22] The interactions between the ions and valence electrons are described by the projector augmented wave (PAW) method.[23−25] Most of the calculations are done at the level of generalized gradient approximation (GGA), employing the exchange-correlation functional by Perdew, Burke, and Ernzerhof (PBE).[26] A plane-wave cutoff energy of 950 eV and a Monkhorst−Pack 5 × 5 × 5 mesh of k points were tested to provide converged results and then used in all the calculations. The total energy criterion for the electronic self-consistency loop was 10^{-6} eV/unit cell, and the structures were fully relaxed (including cell parameters and internal coordinates) until the maximum force acting atoms was below 10^{-5} eV/Å. Static calculations employing the improved linear tetrahedron method[27] were conducted after the geometry optimization to obtain accurate total energies.

Pure density functionals fail to accurately describe van der Waals interactions due to the dynamic nature of the correlations between charge density fluctuations. One approach to work around this problem has been proposed by Grimme,[28] in which the van der Waals interactions are described via a simple pairwise force field optimized for several popular DFT functionals (including PBE). This method, hereafter referred to as DFT-D2, was used in our calculations. Another approach is to adopt a nonlocal correlation functional that approximately accounts for dispersion interactions. On the basis of this approach, several functionals have been developed, of which the original vdW-DF functional[29,30] and optB86b functional[31] are also used in our calculations.

To evaluate the relative thermodynamic stability of cuprous hydroxide, we performed ab initio based modeling of the enthalpy and Gibbs free energy for solid Cu, Cu_2O, and CuOH as well as for gaseous and liquid H_2O and gaseous H_2. For water and hydrogen, all of the thermodynamic contributions (except for the ab initio calculated electronic total energies and zero-point energies of isolated H_2O and H_2 molecules) were taken from the NIST-JANAF thermochemical tables.[32] The electronic total energy was calculated with the PBE functional. Pure DFT has reduced accuracy for some molecular species, and the stability of an H_2 dimer is underestimated by 0.21 eV within the PBE.[33] The PBE energy of H_2 was corrected for that error in our evaluation. The phonon spectra of the solids were calculated on the basis of density functional perturbation theory (DFPT)[34] and the PBE functional implemented in VASP[21,22,35] and post-treated using PHONOPY code.[36] Configurational entropy was taken into account in the thermodynamic calculations.

Experimental Details. Cuprous hydroxide was synthesized by the reduction of Cu^{2+} aqua ions with ferrous ethylenediamine tetraacetate (EDTA).[13,37] A mixture of the disodium salt of EDTA acid, tartaric acid, and caustic soda was gradually mixed first with copper(II) sulfate and then with ferrous sulfate solutions with an approximate volume ratio of 1:1:1. A yellow precipitate formed as a result. The precipitate was filtered, washed with water and ethanol, and dried in air. The pH of the final solution was above 10. All procedures were done in ambient air and at room temperature. Chemicals were provided by Sigma-Aldrich Co. LLC. X-ray diffraction (XRD) patterns were recorded with a PANalytical X'Pert PRO diffraction system (Cu Kα radiation with wavelength λ 1.54 Å) using Bragg−Brentano geometry in the 2θ range 10−100°. Cu_2O powder (of 99% purity industrially produced by Alfa Aesar and Johnson Matthey Co.) was used as a reference sample.

RESULTS AND DISCUSSION

Lifting of the Degeneracy. The calculated energies of all 40 symmetry-distinct configurations of cuprice are plotted in Figure 2 as a function of the displacement between the two

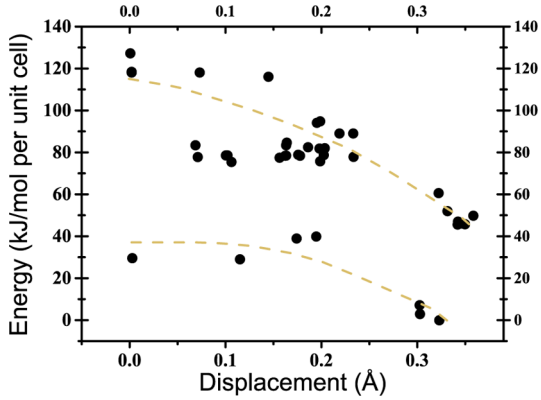

Figure 2. Energy (in kJ per 16 mol of CuOH) of cuprice as a function of the relative displacement (Å) of the two interpenetrating lattices. The energies are calculated by pure DFT at the PBE level, and the displacement is estimated by taking the difference between the centers of mass of the two cubic diamond sublattices of oxygen in the optimized geometry.

lattices, where the zero of the energy is set to the energy of the most stable structure (Figure 3). It will be later discussed why the relative displacement is a suitable parameter to represent the structural differences. The general trend obtained in Figure 2 is that the total energy of cuprice decreases as the displacement increases. Another feature is the gap separating the data, due to which the configurations can be classified into two groups according to their energies. A close inspection reveals that the configurations belonging to the lower energy group share a common feature not typical of the other group: namely, that the low-energy configurations have a clear-cut layered structure with intralayer and interlayer hydrogen bonding and more inner layer Cu atoms. The three-dimensional HB network contributes to the mechanical stability of the structures, imparting stiffness to the material. It is known that metal hydroxides tend to form layered structures. Our results show that CuOH cuprice is not an exception from this rule.

The energy difference between the most and least stable configurations is 7.49 kJ/mol of CuOH as calculated with PBE. Even though the PBE functional usually describes hydrogen-bonding and electrostatic interactions quite well, it fails to

DOI: 10.1021/acs.inorgchem.5b01030
Inorg. Chem. 2015, 54, 8969−8977

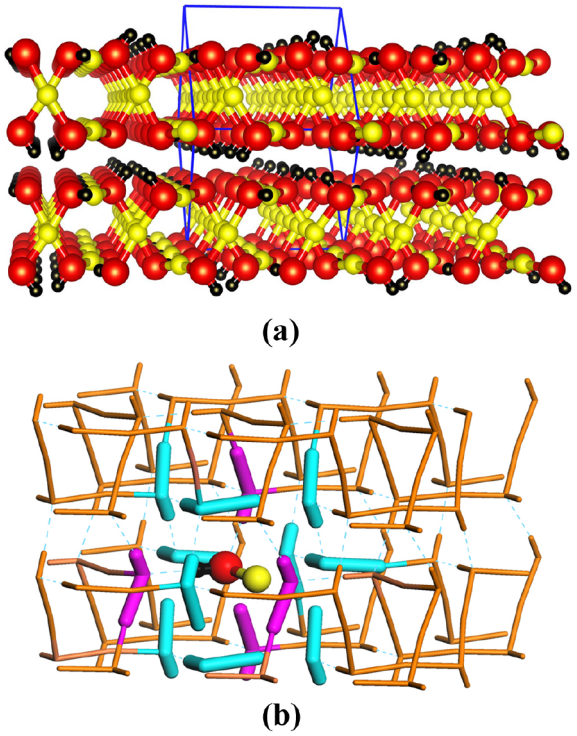

Figure 3. Ball-and-stick representation (a) and stick representation (b) of the ground-state structure of cuprice. In the ball-and-stick model, the red, yellow, and black balls represent O, Cu, and H ions, respectively. The blue frame indicates the supercell. In part b, one CuOH molecule is shown using the ball-and-stick representation, while the surrounding CuOH molecules are colored according to a scheme where the cyan and purple colors indicate different lattices.

describe correlated electron fluctuation and dispersion forces.[38] Given this, we also employed different DFT methods that include van der Waals (vdW) corrections. The calculated energy difference between the most and least stable configurations of cuprice is shown in Table 2, in comparison

Table 2. Energy Difference (in kJ/mol of CuOH or H_2O) between the Most and the Least Stable Configurations of Cuprice and Ice VII/VIII, Obtained with PBE and with Three Dispersion-Corrected DFT Functionals

material	PBE	DFT-D2	vdW-DF	optB86b
CuOH	7.49	6.51	4.91	7.70
H_2O	1.27	1.04	1.18	1.26

with that of ice-VII/VIII. The semiempirical vdW corrected method DFT-D2[28] yields a slightly smaller energy difference in comparison to the value obtained with PBE. The nonlocal embedded vdW correction method of the vdW-DF functional[29,30] gives a smaller energy difference, since it adopts a more repulsive exchange term. The improved nonlocal vdW correction method of optB86b[31] with a less repulsive exchange term gives a larger energy difference. Overall, the PBE functional gives an energy difference similar to that obtained using more sophisticated vdW functionals for the cuprice system as well as for the ice-VII/VIII system. Therefore, the ordering in both systems is more likely to be caused by electrostatic rather than dispersion interactions.

Antiferroelectric Ground State. Figure 3 shows the antiferroelectrically ordered structure that is found to be the ground-state configuration of cuprice. The structure is composed of triple layers (trilayers): a plane of copper atoms (Cu type I) sandwiched between two almost flat layers containing rows of copper (Cu type II), hydrogen, and oxygen atoms. Despite the fact that the inner part of each trilayer is entirely composed of metal atoms, the compound is a semiconductor. Our calculations using the PBE0 hybrid functional[39] yield a band gap value of 3.03 eV, as shown in Figure 4. It is also shown in Figure 4 that the two types of

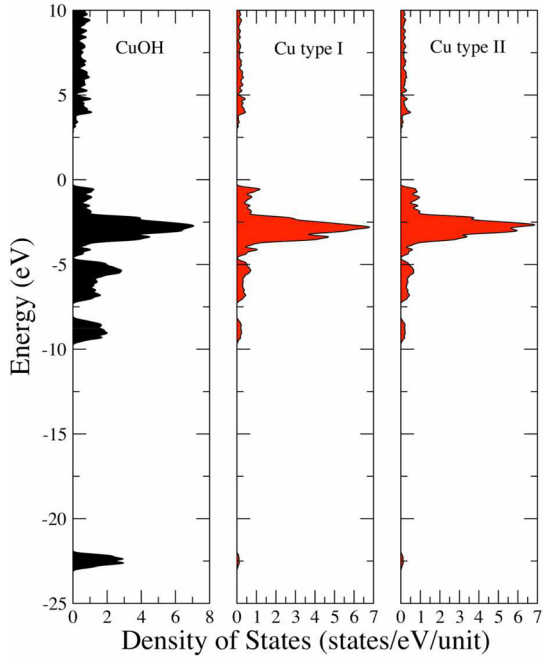

Figure 4. Total DOS (TDOS) of the most stable CuOH and the DOS of the two types of Cu^+, calculated with the PBE0 functional.

copper cations can hardly be distinguished solely by their density of states (DOS). Different ordering of the cations in CuOH affects only slightly the band gap (narrowing it down to 2.73 eV in the cation-disordered cuprice) but never leads to metallicity as long as the Pauling ice rule is obeyed. This feature makes cuprice similar to materials such as topological insulators and graphane-like structures. In addition, this result may be important for understanding the behavior of CuOH surface films, which have been reported to protect metastable copper hydride CuH(s) from reacting with water.[40,41]

The insulating character of CuOH can be understood if one analyzes the topology of primary Cu−O and O−H bonds. Each trilayer resembles a dense fabric woven of two arrays of effectively one-dimensional $[CuOH]_n$ polymer chains. The polymer chains in the one array are coiled into helices, whereas the chains in the other array are folded in a zigzag manner. Neighboring chains belonging to the same array are connected by intralayer hydrogen bonds, whereas the chains belonging to different arrays also belong to different lattices and are therefore disconnected. As a result, the two crossing arrays of polymer chains are not connected by any bonds but are just interlocked together, forming the dense fabric of a trilayer (the assembly is illustrated in Figure 5d). Intralayer HBs are not binding the two arrays together, but they are interwoven around the polymer chains in such a way that the arrays cannot be separated without breaking these bonds.

DOI: 10.1021/acs.inorgchem.5b01030
Inorg. Chem. 2015, 54, 8969−8977

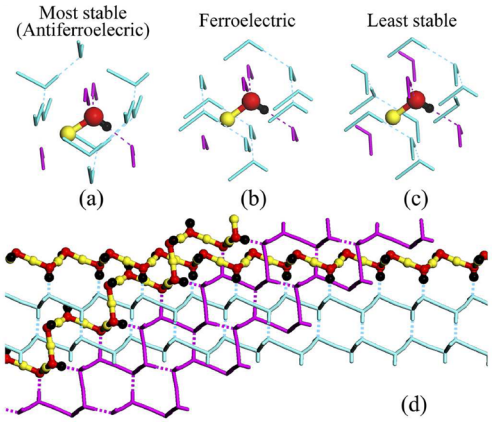

Figure 5. Stick model representations of the configurations of CuOH molecules in the most stable antiferroelectric (a) and ferroelectric (b) structures and the least stable (c) structure of cuprice. In the most stable antiferroelectric configuration, the dipole moments of molecules belonging to the two lattices are antiparallel. Part d shows the two crossing arrays of CuOH molecular chains that are woven together into a trilayer of the most stable structure. The color scheme is the same as in Figure 3.

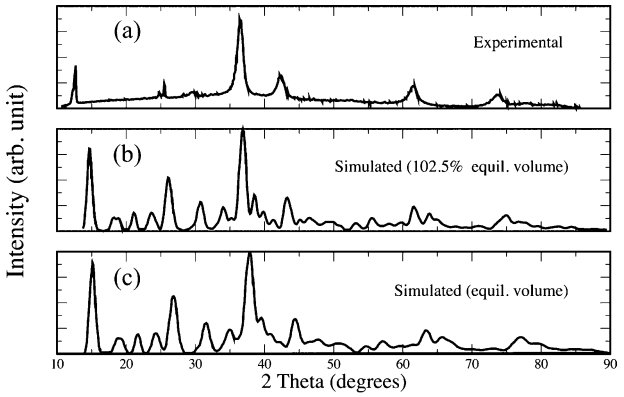

Figure 6. Experimental (a) and simulated (b, c) (on the basis of the structure optimized by the vdW-DF functional) XRD patterns of the cuprice. The XRD simulation was conducted in GDIS code.[45]

The layered ground-state structure implies that individual CuOH trilayers can be intercalated by water spacer layers or even exfoliated, as has been done for the other hydroxides[42] and the layered transition-metal dichalcogenides.[43,44] Indeed, flakes of solid-state cuprous hydroxide, synthesized by the reduction of Cu^{2+} with ferrous ethylendiamine tetraacetate, are stable in water.[13] The possibility of producing freestanding semiconducting nanolayers that are stable in water may be of interest for technological applications.

Comparison with Experiment. The X-ray diffraction pattern (XRD) calculated for the CuOH structure was compared to that obtained from the synthesized yellow CuOH precipitate. The yellow precipitate was obtained by reduction of Cu(II) to Cu(I) in aqueous solution with ferrous ethylendiamine tetraacetate. The details of synthesis are described elsewhere in refs 13 and 37. It is worth noting that the solid CuOH is always poorly crystalline and shows signs of instability. When CuOH forms in water, defects are naturally expected to occur. Because the crystal structure is composed by interlocking together two strands of CuOH polymer chains, it is very easy to entrap water molecules into the structure due to the similarity. Meanwhile, many low-energy cation configurations apart from the most-stable one are also expected to occur in the precipitates. In addition, topological defects such as broken or branching chains can be present in the experimentally investigated structure. On removal from water, decomposition of CuOH to form Cu_2O and H_2O is spontaneous. These circumstances complicate a quantitative comparison between the experimental and the theoretical results.

As seen in Figure 6a, there are peaks at low 2θ angles (12.2 and 24.7°). These peaks indicate the existence of a periodic layered structure with interlayer distances of approximately 7.2 Å. Additionally, at higher 2θ angles (above 29°) the peak positions are almost coincident with those of the Cu_2O reference sample (not shown here)[13] as well as with the calculated peak positions for CuOH (see Figure 6b,c). It can be seen in the figures that the simulated XRD pattern of the ground-state structure of cuprice exhibits peaks similar to those found in the experimental XRD. However, the simulated pattern is shifted toward higher 2θ angles, which correspond to smaller interatomic distances. The first XRD peak (at $2\theta \approx 15°$) of the calculated XRD corresponds to an interatomic distance of 5.7 Å, which is 1.5 Å smaller than that determined from the experimental curve. However, at higher 2θ, the interatomic distances in the calculated structure are just 0.1–0.2 Å shorter than in the experimental structure. This finding indicates that the synthesized sample consists of layers with an intralayer structure possibly composed of structures similar to the DFT-obtained CuOH structure. It should be noted that the space between layers might be filled with water molecules, which is a common phenomenon for metal hydroxides.[46,47] The interlayer water would cause the structure of the compound to expand, thus leading to larger interlayer distances.[46−48] Indeed, in a previous study it was found that the surface composition of the obtained precipitate corresponds to $CuOH{\cdot}H_2O$: i.e., a hydrated form of cuprous hydroxide.[13] There are indications that crystalline water can leave the structure at increased temperatures (in the range from 137 to 160 °C), causing the sample to lose its initial weight by approximately 25%.[13] The thermal expansion can also contribute to a discrepancy between the theoretical and experimental XRD patterns (the simulated XRD was obtained at $T = 0$ K). However, this contribution is less than 0.1 Å.

Nature of Ordering. Interactions between the formally closed shell Cu cations have been argued to be important for the structural stability of cuprite Cu_2O.[49−54] Could these interactions be at the origin of the attractive forces between the two lattices also in CuOH? The differential charge density (which is obtained by subtracting the superimposed electron densities of Cu^+ and O^{2-} ions from the self-consistent or measured charge density of Cu_2O crystal) suggests the existence of an incomplete d shell and on-site 3d−4sp hybridization. Filippetti and Fiorentini[54] showed that the weak Cu−Cu interaction originates from the excessive delocalized charge on Cu and that the incompleteness of the 3d shell is not a direct cause of Cu−Cu interactions. Here, we show that closed-shell interactions do contribute to the bonding between the two lattices present in each of these materials, but they do not produce significant energy differences between the structures of CuOH. These interactions reduce the repulsive force due to the Pauli exclusion principle between closed shells by charge redistribution.

DOI: 10.1021/acs.inorgchem.5b01030
Inorg. Chem. 2015, 54, 8969−8977

We performed the differential charge density calculations for Cu_2O, Li_2O (obtained by substitution of Cu in Cu_2O), CuOH, and ice-VIII. We calculated the differential charge density by subtracting the charge density of the crystal by the superimposed charge densities of the two interpenetrating lattices A and B. This approach allows for a better description of the interactions between the lattices. The differential charge density is given by

$$\rho_D = \rho_{crystal} - (\rho_A + \rho_B) \quad (7)$$

Figure 7 shows the differential charge density plots. All of the structures show charge redistribution, which underscores the correlation of the two interpenetrating lattices. For the cuprous oxide and hydroxide, there is charge accumulation around copper cations and charge removal from the Cu−O bonds and interstitial regions. The charge redistribution strongly depends on the local environment of copper cations. Specifically, it depends on the neighboring copper cations of another lattice. The accumulated charge around copper cations tends to expand toward the nearest copper cations. The charge redistribution around protons is trivial in comparison to copper cations, which is probably due to the small radii and incompleteness of the proton s shell. For the three structures of CuOH, the amount of charge redistribution is similar though the shape is different. In the structures of ice-VIII and Li_2O without copper cations, the charge redistribution is significantly decreased. The main charge redistribution occurs among oxygen anions. In ice-VIII, the charge accumulates in the interstitial region between oxygen anions. However, in Li_2O, the charge accumulates around oxygen anions rather than around cations. This is opposite to what is observed for the other structures. The influences of the interlattice interaction can be summarized as follows.

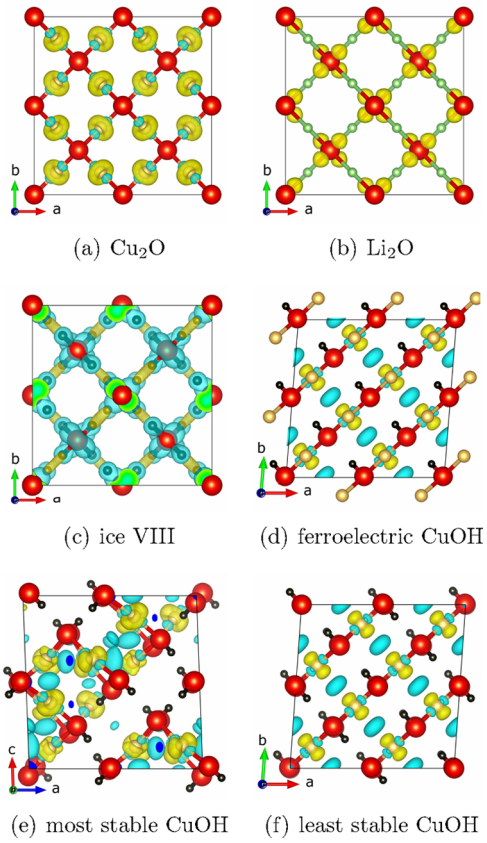

Figure 7. Differential charge density plots (yellow, charge accumulation; cyan, charge depletion): (a) the cuprite Cu_2O; (b) Li_2O; (c) ice-VIII; (d) 2 × 2 × 2 supercell of the CuOH primitive cell; (e) the most stable CuOH configuration; (f) the least stable CuOH configuration. The isosurface value is 0.003 eV/Å^3 for parts a and d−f, 0.00035 eV/Å^3 for part b, and 0.0006 eV/Å^3 for part c, respectively. The total charge accumulations/depletions per cell for parts a−f are 1.74, 0.15, 0.15, 1.03, 1.12, and 1.02 electrons, respectively.

(a) The redistribution of charge density is a result of the correlation between the two interpenetrating lattices.

(b) Copper cations are much more sensitive to such interaction than Li cations and protons. The shape and the amount of charge redistribution depend on the local environment of copper cations.

(c) There is no significant difference on the amount of charge redistribution for the three CuOH structures. Thus, the small difference in charge redistribution cannot account for the large energy difference among the structures of CuOH.

The symmetry of local atomic configurations is generally lower in cuprice than in cuprite, which induces lower-order multipole (dipole) moments on the ions in CuOH and makes the electrostatic attraction (between lattices) much stronger than that in Cu_2O. Furthermore, the interaction is extremely sensitive to the cation arrangements around the oxygen cations and this drives the cation ordering in cuprice. As shown in Figure 3b and Figure 5a, the CuOH molecules in the ground-state structure of cuprice are antiferroelectrically ordered into the same configuration as water molecules in ice-VIII. The axis of antiferroelectric ordering in CuOH lies in-plane not only to minimize the electrostatic interaction between different trilayers but also to maximize the interaction among the CuOH chains within each trilayer, thereby gluing them together.

This interaction, which by nature is a collective electrostatic phenomenon, is also responsible for the lifting of the structural degeneracy in both cuprice and ice-VII/VIII. The interaction is much stronger in cuprice, where it induces a noticeable attraction between the two lattices. In the ground-state cuprice configuration, the centers of mass of the cations belonging to the two lattices are located as far apart as possible to minimize their mutual repulsion. The two lattices become strongly polarized as a result of antiferroelectric ordering (as can be seen from the displacement in Figure 2), to increase the attraction between the cations and anions belonging to different lattices. Interestingly, the least stable structure of cuprice is not the ferroelectric configuration. In the ferroelectric case, the centers of mass of the anions and cations are superimposed when viewed from the axis perpendicular to their main plane of symmetry. This disposition gives rise to an eclipsed arrangement and weakens the Coulomb repulsion with the adjacent lattice. In the least stable configuration the centers of mass of the cations belonging to the two lattices are no longer eclipsed (Figure 5c) but staggered, which maximizes their repulsion. These analyses show that the main driving force for the cation ordering is the collective electrostatic interaction, which polarizes the two interpenetrating lattices. Thus, the relative displacement is a suitable parameter to represent this interaction, as used in Figure 2.

According to the ordering mechanism described above, the other form of solid-state CuOH would be more unlikely to occur. Hydrated cuprous oxide is another possible form of CuOH that has the same average composition in the hydroxide,

DOI: 10.1021/acs.inorgchem.5b01030
Inorg. Chem. 2015, 54, 8969−8977

but the Cu and H cations occupy different lattices: $Cu_2O{\cdot}H_2O$. The crystal structure of hydrated cuprous oxide is depicted in Figure 8. The figure shows two interpenetrating lattices: one is

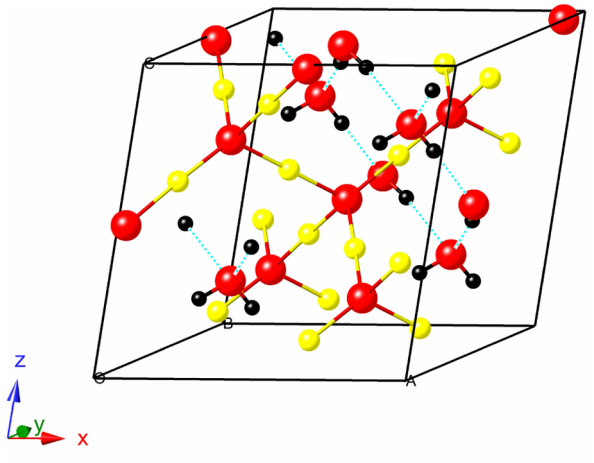

Figure 8. Ball-and-stick model of the crystal structure of the hydrated cuprous oxide.

the anticristobalite lattice of cuprous oxide, and the other is the lattice of cubic ice I_C. The order of protons in the I_C lattice of $Cu_2O{\cdot}H_2O$ corresponds to a ferroelectric configuration, which is the ground state of I_C ice. The total energy of the hydrated cuprous oxide is calculated to be higher than that of the cuprous hydroxide CuOH by 9.86 kJ/mol. The configurational entropy (see Relative Thermodynamic Stability) may additionally contribute 1.36 kJ/mol to the difference at room temperature. This makes the hydrated oxide form less likely to occur in comparison with cuprous hydroxide.

Relative Thermodynamic Stability. The thermodynamics of formation of the lowest-energy configuration of solid CuOH via reactions of Cu or Cu_2O with liquid water have been calculated.

The free energy changes for the following reactions were evaluated:

$$Cu_2O + H_2O \rightarrow 2CuOH$$
$$\Delta H(298.15\ K) = 35.9\ kJ/mol$$
$$\Delta G(298.15\ K) = 46.7\ kJ/mol \quad (8)$$

and

$$Cu + H_2O \rightarrow CuOH + \frac{1}{2}H_2$$
$$\Delta H(298.15\ K) = 80.0\ kJ/mol$$
$$\Delta G(298.15\ K) = 71.4\ kJ/mol \quad (9)$$

Thus, the reaction to form the most stable structure of cuprice from Cu_2O and water requires 17.9 kJ/mol of CuOH. This is in spite of the fact that, to obtain this lower-bound estimate, we combined the energy of the most stable cuprice configuration with the total configurational entropy of CuOH. The formation of CuOH from Cu and water at room temperature requires 80.0 kJ of energy per mole of CuOH. Subtracting reaction 8 from reaction 9 multiplied by 2, we get

$$2Cu + H_2O \rightarrow Cu_2O + H_2$$
$$\Delta H(298.15\ K) = 62.1\ kJ/mol$$
$$\Delta G(298.15\ K) = 48.1\ kJ/mol \quad (10)$$

By comparing the calculated free energy of reaction 10 with experimental data,[32] $\Delta H(298.15\ K) = 57.6$ kJ/mol and $\Delta G(298.15\ K) = 44.6$ kJ/mol, we conclude that the error of the present thermodynamic evaluation is within 8%. The result that the lowest-energy CuOH structure is higher in energy than the two-phase mixture of Cu_2O and H_2O indicates that the obtained structure is not the global energy minimum of the Cu−O−H system at the average composition 1:1:1. However, the obtained CuOH structure can be regarded as a local energy minimum in the configurational space: i.e., as the ground state of cuprous hydroxide (constrained by the cuprice structural model). Indeed, the calculated positive phonon spectrum and the lower energy of CuOH relative to $Cu_2O{\cdot}H_2O$ imply that bulk CuOH is a metastable compound.

The obtained instability of bulk CuOH relative to Cu and water provides additional evidence that the reaction of copper with water is a surface phenomenon. Indeed, the hydroxylation at some copper surfaces is spontaneous.[6,7] However, the further oxidation of the Cu(110) surface is not spontaneous.[4] Water adsorption via a dissociative pathway was observed on Cu(110) and Cu(100).[3,55] Computational studies indicate that stepped copper surfaces have a high affinity for water.[56]

Studies on the Cu(110) surface by Forster et al. have provided us a picture of the H bonding motifs which occur at that surface.[5,6] A study on the pure hydroxyl phase has shown that the OH dimers are often present as pairs or short chains with one dimer pointing in-plane and the next protruding out-of-plane.[6,7] We also note that an outer layer of each trilayer in the cation-ordered configuration of cuprice is structurally similar to a hydroxylated, missing-row reconstructed Cu(110) surface. Thus, the calculated properties of CuOH may be important for many applications where copper metal is in contact with water or moisture: for example, in electronics, fuel cells, hydrogen separation membranes, and canisters for nuclear waste storage.

CONCLUSIONS

In this work we identified the lowest-energy cation configuration in cuprice—CuOH(s)—using a combined theoretical–experimental effort. In the theoretical investigation, employing density functional theory (DFT), we scanned through 40 symmetry-distinct structures that represent the 82944 possible cation configurations in a 48-atom supercell of CuOH and determined the ground-state configuration. We also performed the synthesis of the compound using a method that is capable of yielding high-purity CuOH(s). The structure determined with DFT was validated by comparison with the X-ray diffraction data obtained from the synthesized material. The ground-state CuOH(s) has a layered structure that is stabilized by antiferroelectric cation ordering which, in turn, is caused by collective electrostatic interactions. We calculated the electronic and thermodynamic properties of the cation-ordered CuOH(s) and found that these properties are intimately linked to the topology of the bond network in the material, which is composed of one-dimensional (folded and interlocked chains) and two-dimensional (layers) structural units. The weak bonding between the layers of CuOH(s) indicates that exfoliation of individual layers is possible. The compound is a

DOI: 10.1021/acs.inorgchem.5b01030
Inorg. Chem. 2015, 54, 8969−8977

semiconductor and is capable of forming nanosheets that are stable in water. These properties may render this material interesting for technological applications.

■ ASSOCIATED CONTENT

Supporting Information

The Supporting Information is available free of charge on the ACS Publications website at DOI: 10.1021/acs.inorgchem.5b01030.

Crystallographic data for cuprice (CIF)

■ AUTHOR INFORMATION

Corresponding Author

*P.A.K.: fax, +46-8-790-9193; tel, +46-73-6954960; e-mail, pavelk@kth.se.

Funding

Financial support from the Swedish Nuclear Fuel and Waste Management Company (SKB) and the Swedish Foundation for Strategic Research (SSF, project ALUX) is gratefully acknowledged.

Notes

The authors declare no competing financial interest.

■ ACKNOWLEDGMENTS

The computations were performed on resources provided by the Swedish National Infrastructure for Computing (SNIC) at the National Supercomputer Center (NSC), Linköping, Sweden, and at the PDC Center for High-performance Computing, Stockholm, Sweden.

■ REFERENCES

(1) Henderson, M. A. *Surf. Sci. Rep.* **2002**, *46*, 1−308.
(2) Carrasco, J.; Hodgson, A.; Michaelides, A. *Nat. Mater.* **2012**, *11*, 667−674.
(3) Andersson, K.; Ketteler, G.; Bluhm, H.; Yamamoto, S.; Ogasawara, H.; Pettersson, L. G.; Salmeron, M.; Nilsson, A. *J. Am. Chem. Soc.* **2008**, *130*, 2793−2797.
(4) Lousada, C. M.; Johansson, A. J.; Korzhavyi, P. A. *J. Phys. Chem. C* **2015**, *119*, 14102−14113.
(5) Forster, M.; Raval, R.; Carrasco, J.; Michaelides, A.; Hodgson, A. *Chem. Sci.* **2012**, *3*, 93−102.
(6) Forster, M.; Raval, R.; Hodgson, A.; Carrasco, J.; Michaelides, A. *Phys. Rev. Lett.* **2011**, *106*, 046103.
(7) Hamada, I.; Kumagai, T.; Shiotari, A.; Okuyama, H.; Hatta, S.; Aruga, T. *Phys. Rev. B: Condens. Matter Mater. Phys.* **2012**, *86*, 075432.
(8) Yamada, T.; Tamamori, S.; Okuyama, H.; Aruga, T. *Phys. Rev. Lett.* **2006**, *96*, 036105.
(9) Bojinov, M.; Betova, I.; Lilja, C. *Corros. Sci.* **2010**, *52*, 2917−2927.
(10) Cleveland, C.; Moghaddam, S.; Orazem, M. E. *J. Electrochem. Soc.* **2014**, *161*, C107−C114.
(11) King, F. *Corrosion* **2013**, *69*, 986−1011.
(12) Korzhavyi, P. A.; Soroka, I. L.; Isaev, E. I.; Lilja, C.; Johansson, B. *Proc. Natl. Acad. Sci. U. S. A.* **2012**, *109*, 686−689.
(13) Soroka, I. L.; Shchukarev, A.; Jonsson, M.; Tarakina, N. V.; Korzhavyi, P. A. *Dalton Trans.* **2013**, *42*, 9585−9594.
(14) Pauling, L. *J. Am. Chem. Soc.* **1935**, *57*, 2680−2684.
(15) Singer, S. J.; Kuo, J.-L.; Hirsch, T. K.; Knight, C.; Ojamäe, L.; Klein, M. L. *Phys. Rev. Lett.* **2005**, *94*, 135701.
(16) Kuo, J.-L.; Singer, S. J. *Phys. Rev. E: Stat. Phys., Plasmas, Fluids, Relat. Interdiscip. Top.* **2003**, *67*, 016114.
(17) Gillan, M.; Alfè, D.; Bartók, A.; Csányi, G. *J. Chem. Phys.* **2013**, *139*, 244504.
(18) Macher, M.; Klimeš, J.; Franchini, C.; Kresse, G. *J. Chem. Phys.* **2014**, *140*, 084502.
(19) Nisoli, C.; Moessner, R.; Schiffer, P. *Rev. Mod. Phys.* **2013**, *85*, 1473.
(20) Wang, R. F.; Nisoli, C.; Freitas, R. S.; Li, J.; McConville, W.; Cooley, B. J.; Lund, M. S.; Samarth, N.; Leighton, C.; Crespi, V. H. *Nature* **2006**, *439*, 303−306.
(21) Kresse, G.; Joubert, D. *Phys. Rev. B: Condens. Matter Mater. Phys.* **1999**, *59*, 1758.
(22) Blöchl, P. E. *Phys. Rev. B: Condens. Matter Mater. Phys.* **1994**, *50*, 17953.
(23) Kresse, G.; Furthmüller, J. *Comput. Mater. Sci.* **1996**, *6*, 15−50.
(24) Kresse, G.; Furthmüller, J. *Phys. Rev. B: Condens. Matter Mater. Phys.* **1996**, *54*, 11169.
(25) Kresse, G.; Hafner, J. *Phys. Rev. B: Condens. Matter Mater. Phys.* **1993**, *48*, 13115.
(26) Perdew, J. P.; Burke, K.; Ernzerhof, M. *Phys. Rev. Lett.* **1996**, *77*, 3865−3868.
(27) Blöchl, P. E.; Jepsen, O.; Andersen, O. K. *Phys. Rev. B: Condens. Matter Mater. Phys.* **1994**, *49*, 16223.
(28) Grimme, S. *J. Comput. Chem.* **2006**, *27*, 1787−1799.
(29) Dion, M.; Rydberg, H.; Schröder, E.; Langreth, D. C.; Lundqvist, B. I. *Phys. Rev. Lett.* **2004**, *92*, 246401.
(30) Román-Pérez, G.; Soler, J. M. *Phys. Rev. Lett.* **2009**, *103*, 096102.
(31) Klimeš, J.; Bowler, D. R.; Michaelides, A. *J. Phys.: Condens. Matter* **2010**, *22*, 022201.
(32) Chase, M. W. *NIST-JANAF thermochemical tables*; American Chemical Society: Washington, DC, 1998.
(33) Kurth, S.; Perdew, J. P.; Blaha, P. *Int. J. Quantum Chem.* **1999**, *75*, 889−909.
(34) Baroni, S.; de Gironcoli, S.; Dal Corso, A.; Giannozzi, P. *Rev. Mod. Phys.* **2001**, *73*, 515.
(35) Kresse, G., Marsman, M., Furthmüller, J. *VASP, the guide*; *see* http://cms.mpi.univie.ac.at/vasp/.
(36) Togo, A.; Oba, F.; Tanaka, I. *Phys. Rev. B: Condens. Matter Mater. Phys.* **2008**, *78*, 134106.
(37) Cheng, K. *Anal. Chem.* **1955**, *27*, 1165−1166.
(38) Von Lilienfeld, O. A.; Tavernelli, I.; Rothlisberger, U.; Sebastiani, D. *Phys. Rev. Lett.* **2004**, *93*, 153004.
(39) Perdew, J. P.; Ernzerhof, M.; Burke, K. *J. Chem. Phys.* **1996**, *105*, 9982−9985.
(40) Soroka, I. L.; Tarakina, N. V.; Korzhavyi, P. A.; Stepanenko, V.; Jonsson, M. *CrystEngComm* **2013**, *15*, 8450−8460.
(41) Bennett, E.; Wilson, T.; Murphy, P. J.; Refson, K.; Hannon, A. C.; Imberti, S.; Callear, S. K.; Chass, G. A.; Parker, S. F. *Inorg. Chem.* **2015**, *54*, 2213−2220. PMID: 25671787.
(42) Ma, R.; Sasaki, T. *Acc. Chem. Res.* **2015**, *48*, 136−143. PMID: 25490186.
(43) Oyler, K. D.; Ke, X.; Sines, I. T.; Schiffer, P.; Schaak, R. E. *Chem. Mater.* **2009**, *21*, 3655−3661.
(44) Zhuang, H. L.; Hennig, R. G. *Chem. Mater.* **2013**, *25*, 3232−3238.
(45) Fleming, S.; Rohl, A. *Z. Kristallogr.* **2005**, *220*, 580−584.
(46) Pérez-Ramírez, J.; Abelló, S.; van der Pers, N. M. *J. Phys. Chem. C* **2007**, *111*, 3642−3650.
(47) Pérez-Ramírez, J.; Abelló, S.; van der Pers, N. M. *Chem. - Eur. J.* **2007**, *13*, 870−878.
(48) Klemkaite, K.; Prosycevas, I.; Taraskevicius, R.; Khinsky, A.; Kareiva, A. *Cent. Eur. J. Chem.* **2011**, *9*, 275−282.
(49) Zuo, J.; Kim, M.; O'Keeffe, M.; Spence, J. *Nature* **1999**, *401*, 49−52.
(50) Wang, S.-G.; Schwarz, W. E. *Angew. Chem., Int. Ed.* **2000**, *39*, 1757−1761.
(51) Zuo, J.; O'Keeffe, M.; Kim, M.; Spence, J. *Angew. Chem., Int. Ed.* **2000**, *39*, 3791−3794.
(52) Buljan, A.; Llunell, M.; Ruiz, E.; Alemany, P. *Chem. Mater.* **2001**, *13*, 338−344.
(53) Laskowski, R.; Blaha, P.; Schwarz, K. *Phys. Rev. B: Condens. Matter Mater. Phys.* **2003**, *67*, 075102.
(54) Filippetti, A.; Fiorentini, V. *Phys. Rev. B: Condens. Matter Mater. Phys.* **2005**, *72*, 035128.

DOI: 10.1021/acs.inorgchem.5b01030
Inorg. Chem. 2015, 54, 8969−8977

(55) Wang, G.-C.; Nakamura, J. *J. Phys. Chem. Lett.* **2010**, *1*, 3053−3057.
(56) Tang, Q.-L.; Chen, Z.-X. *Surf. Sci.* **2007**, *601*, 954−964.

DOI: 10.1021/acs.inorgchem.5b01030
Inorg. Chem. 2015, 54, 8969−8977